Spiro-silacycloalkyl Tetraphenylsiloles with a Tunable Exocyclic Ring: Preparation, Characterization, and Device Application of 1,1′-Silacycloalkyl-2,3,4,5-tetraphenylsiloles

Ho-Jin Son,† Won-Sik Han,† Ji-Yun Chun,† Chan-Jae Lee,‡ Jung-In Han,‡ Jaejung Ko,*,† and Sang Ook Kang*,†

Department of Chemistry, Korea University, 208 Seochang, Chochiwon, Chung-nam 339-700, Korea, and Information Display Research Center, Korea Electronics Technology Institute, 68 Yatap-dong, Bundang-gu, Seongnam-si, Gyeonggii-do, 463-816, Korea

Received September 18, 2006

A series of 2,3,4,5-tetraphenylsiloles (**3**), with a four- to six-membered silacyclo alkyl substituent at the 1,1′-position, have been prepared by a one-pot synthesis of dilithium diyne (**2**) with the corresponding silacycloalkyl dichlorosilane precursors (**1**). The structures of the resulting 1,1′-(silacyclopentenyl)silole (**3b**) and 1,1′-(silacyclopentyl)silole (**3c**) species were studied using X-ray crystallography to obtain geometrical information on exocyclic siloles. Due to the formation of silacyclopentenyl and -pentyl rings, the phenyl substituents on the silole adopted a paddle-wheel conformation to reduce steric hindrance between substituents. The photophysical properties of the silacycloalkyl siloles (**3**) were examined to elucidate the structure−photophysical property relationship arising from variation of the exocyclic ring size. Indeed, the size of the exocyclic silacycloalkyl ring at the 1,1′-position affected the maximum peaks in the absorption and emission spectra, with systematic blue shifts being observed with increasing exocyclic ring size. A sequential elevation of the LUMO levels was monitored by observing increases in the reduction potential, as seen in the cyclic voltammograms (CVs), with increasing exocyclic ring size. In addition, due to the formation of exocyclic rings, an enhanced thermal stability was observed on the basis of DSC measurements, showing that silacyclopentylsilole (**3c**) exhibits the highest T_g value in the series. Indeed, a three-layer device comprising *N*,*N*′-bis(1-naphthyl)-*N*,*N*′-diphenylbenzidine (NPB) as the hole-transport layer, **3c** as the emitting layer, and Alq_3 as the electron-transport layer displayed a brightness of 11 000 cd/m^2 at 11 V with a current efficiency of 2.71 cd/A.

Introduction

Siloles have unique electronic and photophysical properties.[1] The blue emission with high quantum efficiency and low-lying LUMO energy level of the silole ring (due to $\sigma^*-\pi^*$ conjugation between the σ^* orbital of the exocyclic σ bonds on the silicon and the π^* orbital of the butadiene moiety)[2] make siloles ideal candidates for use as emitting[3] and electron-transporting (ET) materials[4,5] in light-emitting devices (LEDs). Many studies have examined the electronic structure and origin of the photophysical properties of siloles, mainly by use of the inductive effect of the 1,1′-substituents[6] and the π-conjugation effect of the 2,5-substituents.[7] However, few investigations have sought to use geometric effects on the silicon atom to modify the properties of siloles.[8] To this end, we have studied the structure−photophysical property relationship of the silacyclo-

* Corresponding author. Tel: +82-41-860-1334. Fax: +82-41-867-5396. E-mail: sangok@korea.ac.kr.

† Korea University.

‡ Korea Electronics Technology Institute.

(1) (a) Lee, S. H.; Jang, B.-B.; Kafafi, Z. H. *J. Am. Chem. Soc.* **2005**, *127*, 9071. (b) Boydston, A. J.; Yin, Y.; Pagenkopf, B. L. *J. Am. Chem. Soc.* **2004**, *126*, 3724. (c) Xu, C.; Wakamiya, A.; Yamaguchi, S. *Org. Lett.* **2004**, *6*, 3707. (d) Kim, W.; Palilis, L.; Uchida, M.; Kafafi, Z. H. *Chem. Mater.* **2004**, *16*, 4681. (e) Hissler, M.; Dyer, P. W.; Réau, R. *Coord. Chem. Rev.* **2003**, *244*, 1. (f) Roques, N.; Gerbier, P.; Sutter, J.-P.; Guionneau, P.; Luneau, D.; Guérin, C. *Organometallics* **2003**, *22*, 4833. (g) Yamaguchi, S.; Tamao, K. *J. Organomet. Chem.* **2002**, *653*, 223. (h) Losehand, U.; Mitzel, N. W. *J. Chem. Soc., Dalton Trans.* **2000**, 1049. (i) Tamao, K.; Yamaguchi, S. *J. Organomet. Chem.* **2000**, *611*, 5. (j) Adachi, A.; Yasuda, H.; Sanji, T.; Sakurai, H.; Okita, K. *J. Lumin.* **2000**, *87-89*, *1174*, 87−89. (k) Yamaguchi, S.; Jin, R.-Z.; Tamao, K. *J. Am. Chem. Soc.* **1999**, *121*, 2937. (l) Sohn, H.; Huddleston, R. R.; Powell, D. R.; West, R. *J. Am. Chem. Soc.* **1999**, *121*, 2935. (m) Sanji, T.; Sakai, T.; Kabuto, C.; Sakurai, H. *J. Am. Chem. Soc.* **1998**, *120*, 4552. (n) Yamaguchi, S.; Tamao, K. *J. Chem. Soc., Dalton Trans.* **1998**, 3693. (o) Yamaguchi, S.; Jin, R.-Z.; Tamao, K. *Organometallics* **1997**, *16*, 2486. (p) Tamao, K.; Yamaguchi, S.; Shiro, M. *J. Am. Chem. Soc.* **1994**, *116*, 11715. (q) Colomer, E.; Corriu, R. J. P.; Lheureux, M. *Chem. Rev.* **1990**, *90*, 265.

(2) (a) Chan, L. H.; Lee, R. H.; Hsieh, C. F.; Yeh, H. C.; Chen, C. T. *J. Am. Chem. Soc.* **2002**, *124*, 6469. (b) Chan, L. H.; Yeh, H. C.; Chen, C. T. *Adv. Mater.* **2001**, *13*, 1637. (c) Tamao, K.; Ohno, S.; Yamaguchi, S. *Chem. Commun.* **1996**, 1873. (d) Tamao, K.; Yamaguchi, S.; Ito, Y.; Matsuzaki, Y.; Yamabe, T.; Fukushima, M. *Macromolecules* **1995**, *28*, 8668. (e) Khabashesku, V. N.; Balaji, V.; Boganov, S. E.; Nefedov, O. M.; Michl, J. *J. Am. Chem. Soc.* **1994**, *116*, 320.

(3) (a) Chen, H.; Chen, J.; Qiu, C.; Tang, B. Z.; Wong, M.; Kwok, H.-S. *IEEE J. Select. Top. Quantum Electron.* **2004**, *10*, 10. (b) Chen, J.; Law, C. C. W.; Lam, J. W. Y.; Dong, Y.; Lo, S. M. F.; Williams, I. D.; Zhu, D.; Tang, B. Z. *Chem. Mater.* **2003**, *15*, 1535. (c) Palilis, L. C.; Murata, H.; Uchida, M.; Kafafi, Z. H. *Org. Electron.* **2003**, *4*, 113. (d) Chen, H. Y.; Lam, W. Y.; Luo, J. D.; Ho, Y. L.; Tang, B. Z.; Zhu, D. B.; Wong, M.; Kwok, H. S. *Appl. Phys. Lett.* **2002**, *81*, 574. (e) Murata, H.; Kafafi, Z. H.; Uchida, M. *Appl. Phys. Lett.* **2002**, *80*, 189. (f) Luo, J.; Xie, Z.; Lam, J. W. Y.; Cheng, L.; Chen, H.; Qiu. C.; Kwok, H. S.; Zhan, X.; Liu, Y.; Zhu, D.; Tang, B. Z. *Chem. Commun.* **2001**, 1740. (g) Tang, B. Z.; Zhan, X.; Yu, G.; Lee, P. P. S.; Liu, Y.; Zhu, D. *J. Mater. Chem.* **2001**, *11*, 2974.

(4) (a) Palilis, L. C.; Uchida, M.; Kafafi, Z. H. *IEEE J. Select. Top. Quantum Electron.* **2004**, *10*, 79. (b) Risko, C.; Kushto, G. P.; Kafafi, Z. H.; Brédas, J. L. *J. Chem. Phys.* **2004**, *121*, 9031. (c) Palilis, L. C.; Mäkinen, A. J.; Uchida, M.; Kafafi, Z. H. *Appl. Phys. Lett.* **2003**, *82*, 2209. (d) Murata, H.; Kafafi, Z. H.; Uchida, M. *Appl. Phys. Lett.* **2002**, *80*, 189. (e) Uchida, M.; Izumizawa, T.; Nakano, T.; Yamaguchi, S.; Tamao, K.; Furukawa, K. *Chem. Mater.* **2001**, *13*, 2680. (f) Murata, H.; Malliaras, G. G.; Uchida, M.; Shen, Y.; Kafafi, Z. H. *Chem. Phys. Lett.* **2001**, *339*, 161. (g) Tamao, K.; Uchida, M.; Izumizawa, T.; Fukukawa, K.; Yamaguchi, S. *J. Am. Chem. Soc.* **1996**, *118*, 11974.

10.1021/om060854d CCC: $37.00
Publication on Web 12/10/2006

Chart 1. New Types of Exocyclic Silacycloalkyltetraphenyl Siloles (3)

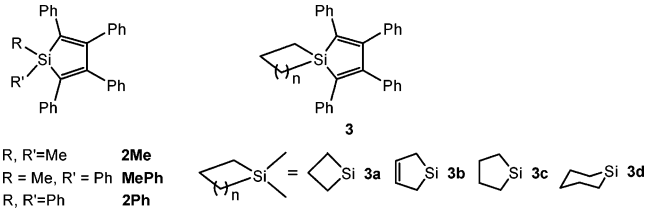

alkyl siloles while varying the exocyclic ring size. We synthesized tetraphenyl siloles substituted with a series of exocyclic rings on the silicon atom and systematically studied their electronic and photophysical properties. Variation of the exocyclic ring size appears to be an origin of the characteristic expansion of the band gap; that is, the larger the ring size, the wider the band gap. In addition, these siloles exhibited enhanced thermal stability due to the formation of an exocyclic spiro-type compound. Here we report the full details of their syntheses and characterizations, together with the crystal structures of **3b** and **3c**. The electronic and photophysical properties of these siloles were studied by means of UV and PL spectroscopy as well as cyclic voltammetry (CV). Furthermore, theoretical calculations for this unique series of siloles were performed to account for the origin of the geometric changes on the silicon atom, as shown in Chart 1.

Results and Discussion

Synthesis of Exocyclic Silacycloalkyltetraphenyl Siloles. Our synthetic route to the 2,3,4,5-tetrasubstituted phenyl siloles (**3**) is shown in Scheme 1.[3g,9]

The 1,4-diphenylbutadiene-1,4-dianion (**2**) generated from diphenylacetylene and Li metal in THF was allowed to react with silacycloalkyl dichlorides (**1**) to give the exocyclic silacycloalkyl siloles (**3**) in moderate yields (47−60%). In all cases, the siloles were isolated by flash chromatography. The formation of exocyclic siloles (**3**) was confirmed by means of high-resolution mass spectrometry and elemental analyses. Each silole showed the expected signals in the ^{1}H and ^{13}C NMR spectra, revealing characteristic exocyclic silacycloalkyl and silole phenyl groups (see Experimental Section).

Scheme 1. Preparation of New Types of Exocyclic Silacycloalkyltetraphenyl Siloles (3)

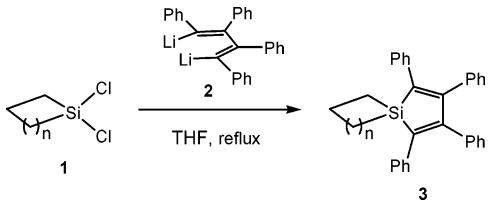

Crystal Structure and Thermal Stability of Silole Derivatives (3). The solid-state structures of 1,1′-(silacyclopentenyl)-silole (**3b**) and 1,1′-(silacyclopentyl)silole (**3c**) derived from single-crystal X-ray analyses revealed that these compounds are both isomorphous and isostructural. The exocyclic silacycloalkyl ring anchors the 1,1′-silicon atom of the silole, forming the expected spiro compound (Figure 1). Their crystal data are summarized in Table 1, and selected bond distances and angles are listed in Table 2. The crystal structures of siloles **3b** and **3c** exhibit phenyl groups with highly twisted conformations at the ring carbons in the silole skeleton. Each structure displays a propeller-like arrangement of the four phenyl rings and exocyclic silacycloalkyl ring. The tetraphenyl rings are twisted out of the central silole ring; the twisted angles between the four phenyl groups and the silole ring are −37.0° to −66.5° for **3b** and −42.4° to −65.4° for **3c**. These values are similar to those found in 1,1′-(dimethyl)silole (**2Me**) and 1,1′-(methylphenyl)silole (**MePh**).[6b] The formation of the silacycloalkyl ring gives rise to constraints on the adjacent four phenyl groups of the silole ring. These siloles contain an almost planar silole ring with torsional angles less than 2.4°, having a silacyclopentenyl silole (**3b**) with a better planarity than silacyclopentyl silole (**3c**). The endocyclic C−C (single) and C═C (double) bond lengths are within the range of normal values (mean C−C 1.51 vs C═C 1.36 Å) found in other silole derivatives such as **2Me**, **MePh**, and **2Ph**, while the exocyclic Si−C bond lengths are comparable to those of the endocyclic Si−C bonds (within the range of 1.87 Å). Compared with 1,1′-(dimethyl)silole (**2Me**), the exocyclic Si−C bonds in **3b** and **3c** are somewhat stretched due to the cyclization effect of the silacycloalkyl group. The average endocyclic and exocyclic C−Si−C bond angles of **3b** and **3c** are 92.3° and 95.2°, respectively. Again, such constrained tetrahedral angles around the silicon atom are due to the formation of a spiro-type geometry. In noncyclic 1,1′-substituted siloles (**2Me**, **MePh**, and **2Ph**), the exocyclic C−Si−C bond angle (108.98−111.6°) is larger than the endocyclic C−Si−C bond angle (92.19−93.20°).

In the packed model of **3c**, the bow-tie shape of the exocyclic ring induces compact packing in the solid-state structure, leading to an efficient intermolecular $\pi-\pi$ overlap (Figure 2). Looking down along the *x*-axis, **3c** shows a shorter interlayer distance than that of **MePh** (5.39 vs 5.63 Å). More importantly, **3c** forms a long-range band structure along the *z*-axis. Tethering the 1,1′-position of the silicon atom on the silole enables the formation of a better layered structure than **MePh** in the solid packing. A similar result was reported by Yin et al., which suggests that the intermolecular $\pi-\pi$ overlap depends on the steric hindrance of the 1,1′-position on silicon.[10]

The thermal stability of the siloles (**3**) was measured using differential scanning calorimetry (DSC). As shown in Table 3, enhanced thermal stability was observed in the following series: the silole derivatives (**3b**−**d**) exhibit a M_p of 208−220

(5) (a) Ohshita, J.; Kai, H.; Sumida, T.; Kunai, A.; Adachi, A.; Sakamaki, K.; Okita, K. *J. Organomet. Chem.* **2002**, *642*, 137. (b) Ohshita, J.; Kai, H.; Takada, A.; Iida, T.; Kunai, A.; Ohta, N.; Komaguchi, K.; Shiotani, M.; Adachi, A.; Sakamaki, K.; Okita, K. *Organometallics* **2001**, *20*, 4800. (c) Ohshita, J.; Nodono, M.; Kai, H.; Watanabe, T.; Kunai, A.; Komaguchi, K.; Shiotani, M.; Adachi, A.; Okita, K.; Harima, Y.; Yamashita, K.; Ishikawa, M. *Organometallics* **1999**, *18*, 1453.

(6) (a) Zhan, X.; Risko, C.; Amy, F.; Chan, C.; Zhao, W.; Barlow, S.; Kahn, A.; Brédas, J. L.; Marder, S. R. *J. Am. Chem. Soc.* **2005**, *127*, 9021. (b) Yu, G.; Yin, S.; Liu, Y.; Chen, J.; Xu, X.; Sun, X.; Ma, D.; Zhan, X.; Peng, Q.; Shuai, Z.; Tang, B. Z.; Zhu, D.; Fang, W.; Luo, Y. *J. Am. Chem. Soc.* **2005**, *127*, 6335. (c) Yamaguchi, S.; Jin, R.-Z.; Tamao, K. *J. Organomet. Chem.* **1998**, *559*, 73.

(7) (a) Lee, J.; Liu, Q.-D.; Bai, D.-R.; Kang, Y.; Tao, Y.; Wang, S. *Organometallics* **2004**, *23*, 6205. (b) Lee, J.; Liu, Q.-D.; Motala, M.; Dane, J.; Gao, J.; Kang, Y.; Wang, S. *Chem. Mater.* **2004**, *16*, 1689. (c) Yamaguchi, S. Goto, T.; Tamao, K. *Angew. Chem., Int. Ed.* **2000**, *39*, 1695. (d) Yamaguchi, S.; Endo, T.; Uchida, M.; Izumizwa, T.; Furukawa, K.; Tamao, K. *Chem. Eur. J.* **2000**, 1683. (e) Lee, Y.; Sadki, S.; Tsuie, B.; Reynolds, J. R. *Chem. Mater.* **2001**, *13*, 2234. (f) Yamaguchi, S.; Jin, R.-Z.; Ohno, S.; Tamao, K. *Organometallics* **1998**, *17*, 5133. (g) Katkevics, M.; Yamaguchi, S.; Toshimitsu, A.; Tamao, K. *Organometallics* **1998**, *17*, 5796. (h) Yamaguchi, S.; Jin, R.-Z.; Tamao, K.; Sato, F. *J. Org. Chem.* **1998**, *63*, 10060. (i) Yamaguchi, S.; Jin, R.-Z.; Tamao, K. *Organometallics* **1997**, *16*, 2230.

(8) (a) Resibois, B.; Brunet, J. C. *Ann. Chim.* **1970**, *5*, 199. (b) Resibois, B.; Hode, C.; Picart, B.; Brunet, J. C. *Ann. Chim.* **1969**, *4*, 203.

(9) (a) Curtis, M. D. *J. Am. Chem. Soc.* **1969**, *91*, 6011. (b) Braye, E. H.; Hubel, W.; Caplier, I. *J. Am. Chem. Soc.* **1961**, *83*, 4406.

(10) Yin, S.; Yi, Y.; Li, Q.; Yu, G.; Liu, Y.; Shuai, Z. J. Phys. *Chem. A* **2006**, *110*, 7138.

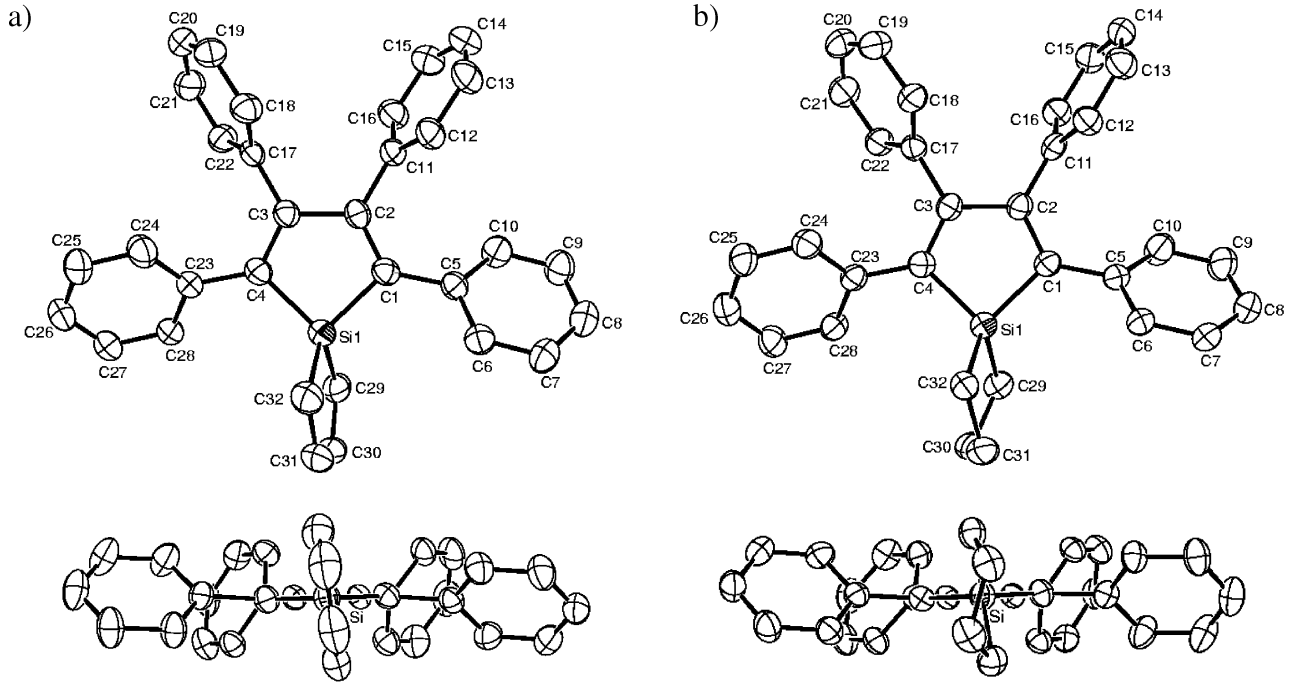

Figure 1. ORTEP drawing (30% probability for thermal ellipsoids) of (a) **3b** and (b) **3c**. Hydrogen atoms are omitted for clarity.

Table 1. Crystal data and structure refinement for 3b and 3c

	3b	**3c**
empirical formula	$C_{32}H_{26}Si$	$C_{32}H_{28}Si$
fw	438.65	440.66
temperature	293(2) K	293(2) K
wavelength	0.71073 Å	0.71073 Å
cryst syst, space group	orthorhombic, Pbca	orthorhombic, *Pbca*
unit cell dimens	$a = 19.0687(11)$ Å, $\alpha = 90°$	$a = 18.806(5)$ Å, $\alpha = 90°$
	$b = 10.6623(6)$ Å, $\beta = 90°$	$b = 10.791(3)$ Å, $\beta = 90°$
	$c = 24.3172(14)$ Å, $\gamma = 90°$	$c = 24.623(6)$ Å, $\gamma = 90°$
volume	4944.1(5) Å^3	4997(2) Å^3
Z, calcd density	8, 1.179 mg/m^3	8, 1.171 mg/m^3
μ	0.112 mm^{-1}	0.111 mm^{-1}
$F(000)$	1856	1872
cryst size	0.32 × 0.20 × 0.18 mm	0.25 × 0.11 × 0.09 mm
θ range for data collection	1.99−28.33°	1.65−28.28°
limiting indices	$-25 \le h \le 25$	$-25 \le h \le 25$
	$-14 \le k \le 14$	$-14 \le k \le 14$
	$-32 \le l \le 32$	$-32 \le l \le 32$
no. of reflns collected/unique	48 784/6162 [R(int) = 0.0473]	64 748/6203 [R(int) = 0.0898]
max. and min. transmn	0.9796 and 0.9654	0.9906 and 0.9732
refinement method	full-matrix least-squares on F^2	full-matrix least-squares on F^2
no. of data/restraints/params	6162/0/298	6203/0/299
goodness-of-fit on F^2	1.043	1.054
final R indices [$I > 2\sigma(I)$]	$R_1 = 0.0512$, $wR_2 = 0.1271$	$R_1 = 0.0600$, $wR_2 = 0.1486$
R indices (all data)	$R_1 = 0.1197$, $wR_2 = 0.1815$	$R_1 = 0.1515$, $wR_2 = 0.2223$
largest diff peak and hole	0.245 and −0.279 e Å^{-3}	0.306 and −0.360 e Å^{-3}

[a] $R_1 = \sum||F_o| - |F_c||$ (based on reflections with $F_o^2 > 2\sigma F^2$. [b] $wR_2 = [\sum[w(F_o^2 - F_c^2)^2]/\sum[w(F_o^2)^2]]^{1/2}$; $w = 1/[\sigma^2(F_o^2) + (0.095P)^2]$; $P = [\max(F_o^2, 0) + 2F_c^2]/3$ (also with $F_o^2 > 2\sigma F^2$).

°C and a T_g of 83−91 °C, which are higher than the values for the acyclic compounds (**2Me**, **MePh**, and **2Ph**). On the basis of these data, we speculate that the spiro-type structure imparts extra thermal stability to silacycloalkyl siloles.

Photophysical Properties of Silole Derivatives (3). The UV−visible absorption and fluorescence spectra of the silacycloalkylsiloles (**3**) were measured in chloroform and in the corresponding solid film, and the resulting spectral data are summarized in Table 3. In the UV−visible absorption spectra, the position of the absorption maximum (ca. 360 nm) ascribed to the $\pi-\pi^*$ transition of the silacyclopentadiene ring depends significantly on the size of the 1,1′-substituted silacycloalkyl ring. Specifically, increasing the ring size leads to a blue shift

Table 2. Selected Bond Lengths and Angles of 3b and 3c

length (Å)	**3b**	**3c**	angle (deg)	**3b**	**3c**
Si1−C1	1.871(2)	1.878(3)	Si1−C1−C2	107.6(2)	107.5(2)
Si1−C4	1.874(3)	1.868(3)	Si1−C4−C3	107.4(2)	108.4(2)
C1−C2	1.349(3)	1.366(4)	C4−C3−C2	116.2(2)	115.8(3)
C2−C3	1.504(3)	1.507(4)	C3−C2−C1	116.4(2)	116.1(3)
C3−C4	1.358(3)	1.357(4)	C4−Si1−C1	92.4(1)	92.2(1)
Si1−C29	1.866(3)	1.874(4)	C29−Si1−C32	95.5(2)	94.8(2)
Si1−C32	1.875(3)	1.868(3)	C24−C23−C4−C3	−37.6(4)	−42.9(5)
C4−C23	1.482(3)	1.479(4)	C18−C17−C3−C2	−66.5(3)	−59.5(4)
C3−C17	1.469(3)	1.495(4)	C16−C11−C2−C3	−65.2(3)	−65.4(4)
C2−C11	1.496(3)	1.463(4)	C10−C5−C1−C2	−37.0(4)	−42.4(5)
C1−C5	1.474(3)	1.474(4)	Si1−C1−C2−C3	1.1(3)	2.1(3)
			C1−C2−C3−C4	−1.6(3)	−2.4(4)

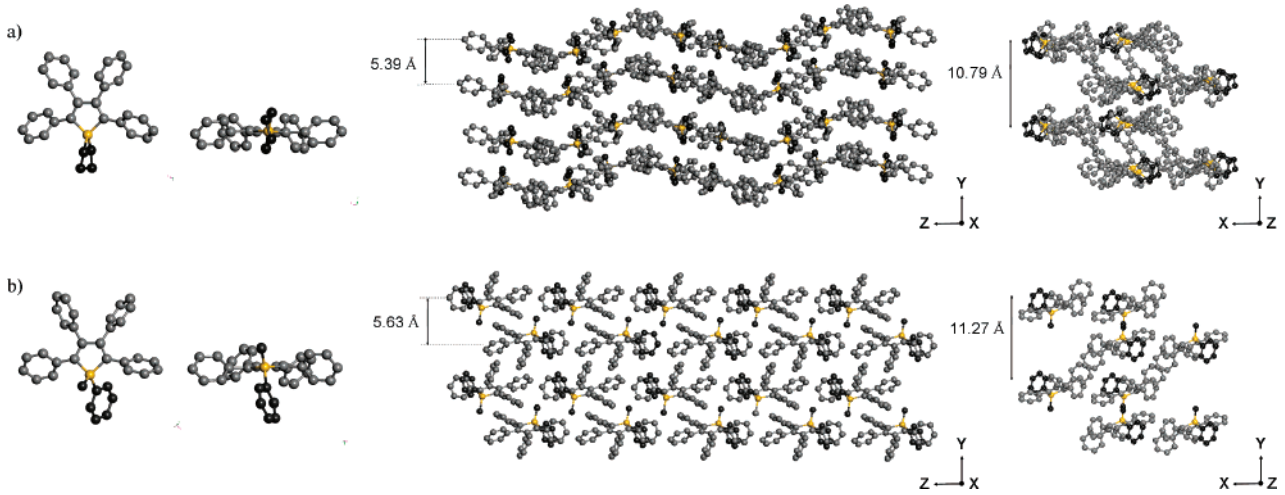

Figure 2. Packed structure in the crystal lattice of (a) **3c** and (b) **MePh**: carbon (gray); silicon (yellow); silacyclopentyl ring and methyl, phenyl moiety on silicon (black).

Table 3. UV−Vis, Photoluminescence Spectral, and Thermal Data for Siloles (3)

		photoluminescence				
silole	UV−vis[a]	solution[a]	film[b]	Φ_f (%)[c]	M_p (°C)	T_g (°C)
3a	373	490	508	0.13	172	
3b	372	481	501	0.24	215	83
3c	366	477	491	0.27	220	91
3d	351	469	481	0.11	208	85
2Me	361	470	481	0.19	177−178	
MePh	363	471	491	0.15	170−171	54[d]
2Ph	366	471	495	0.29	186−187	65[d]

[a] In chloroform. [b] Emission maximum for thin solid film. [c] Relative to 9,10-diphenylanthracene in chloroform at ambient temperature. [d] Reference 6b

of the absorption maximum from 373 nm for **3a** to 351 nm for **3d**, as seen in Table 3. This result provides clear evidence of the geometric effects on the electronic structure of exocyclic siloles. The emission maxima also significantly depend on the size of the 1,1′-substituted exocyclic silacycloalkyl ring, showing a trend similar to that observed in the absorption behavior: the wavelength of PL in the solid film shows a blue shift of about 30 nm as the exocyclic ring size is increased. However, the PL quantum yields in solution were low due to the intramolecular rotation of the phenyl rings, as observed in other silole derivatives such as **2Me**, **MePh**, and **2Ph**. For all of the silole derivatives considered, the measured lifetime at room temperature was about 10−15 ns, with a negligibly long-decay trace. These lifetimes indicate that all of the silole derivatives are fluorescence emitters.

Electrochemistry. Cyclic voltammetry (CV) has been applied to determine the HOMO and LUMO levels of organic compounds, particularly in the area of developing electroluminescent materials. For example, CV has been widely used as a simple and practical tool for optimizing the device structure in organic light-emitting diodes (OLEDs). For this reason, we performed CV studies to determine the HOMO and LUMO levels of the silole series (**3a**−**d**). All of the exocyclic silole compounds exhibited irreversible oxidation and reduction waves, as observed in other silole derivatives such as **2Me**, **MePh**, and **2Ph** (Figure 5).[11] The measurements, which were calibrated using a ferrocene (4.8 eV below the vacuum level)[12] standard, are listed in Table 4. From the first oxidation and reduction potential, the HOMO

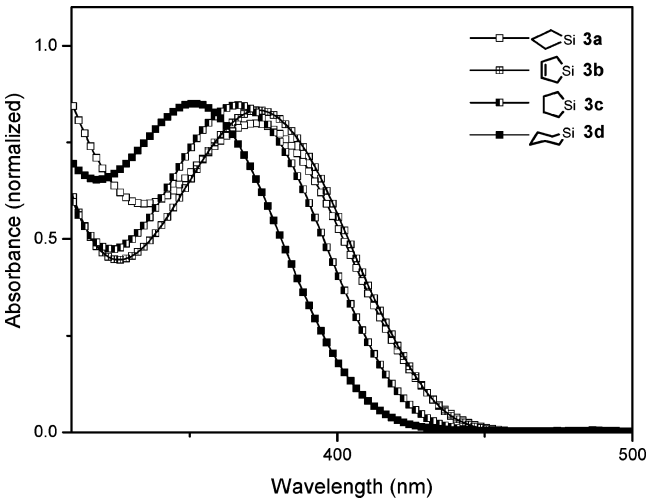

Figure 3. UV−vis absorption spectra of silacycloalkylsiloles (**3**) in chloroform.

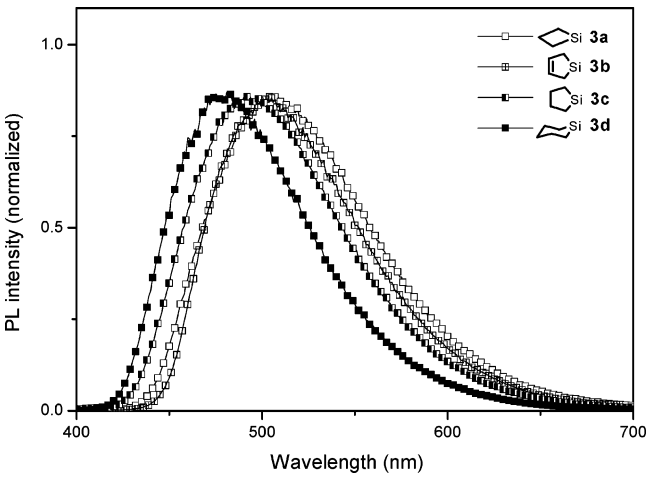

Figure 4. Photoluminescence spectra of silacycloalkylsiloles (**3**) in a thin solid film.

and LUMO energy levels of the siloles were estimated to be −5.53 to ca. −5.48 and −2.55 to ca. −2.32 eV, respectively. These results indicate that the LUMO levels increase systematically in the order **3a** < **3b** < **3c** < **3d** as the size of the

(11) Ferman, J.; Kakareka, J. P.; Klooster, W. T.; Mullin, J. L.; Quattrucci, J.; Ricci, J. S.; Tracy, H. J.; Vining, W. J.; Wallace, S. *Inorg. Chem.* **1999**, *38*, 2464.

(12) Pommerehne, J.; Vestweber, H.; Guss, W.; Mahrt, R. F.; Bassler, H.; Porsch, M.; Baub, J. *Adv. Mater.* **1995**, *7*, 551.

Table 4. Oxidation and Reduction Potentials of Silacycloalkylsiloles (3)

	oxidation (V)[a]		reduction (V)[a]					
compound	E_{pa}	E_{onset}^{ox}	E_{pc}	E_{onset}^{red}	E_g^{el} (eV)[b]	E_g^{opt} (eV)[c]	HOMO (eV)[d]	LUMO (eV)[d]
3a	0.89	0.73	−2.39	−2.25	2.98	2.86	−5.53	−2.55
3b	0.94	0.70	−2.47	−2.31	3.01	2.86	−5.5	−2.49
3c	0.84	0.66	−2.53	−2.38	3.04	2.94	−5.46	−2.42
3d	0.86	0.68	−2.71	−2.48	3.16	3.05	−5.48	−2.32
Alq$_3$[e]	0.73[e]	0.57	−2.30[e]	−2.21	2.78	2.80	−5.37	−2.59

[a] E_{pa} = anodic peak potential; E_{pc} = cathodic peak potential; E_{onset} = onset potential. [b]Electrochemical band gap E_g^{el}. [c]Optical band gap E_g^{opt} from the absorption edge. [d]HOMO and LUMO levels were determined using the following equations: E_{HOMO} (eV) = $-e(E_{onset}^{ox} + 4.8)$, E_{LUMO} (eV) = $-e(E_{onset}^{red} + 4.8)$. [e]Reference 14.

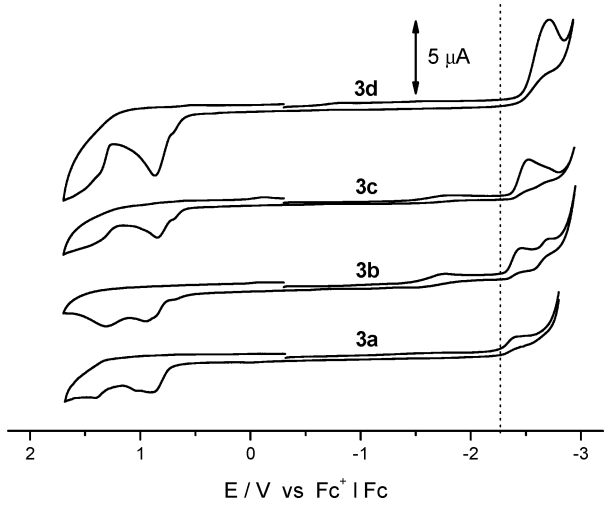

Figure 5. Cyclic voltammograms of 1 mM silacycloalkylsiloles (**3**) at the platinum disk electrode; in CH_2Cl_2 containing 0.1 M Bu_4NClO_4; υ = 0.1 V/s.

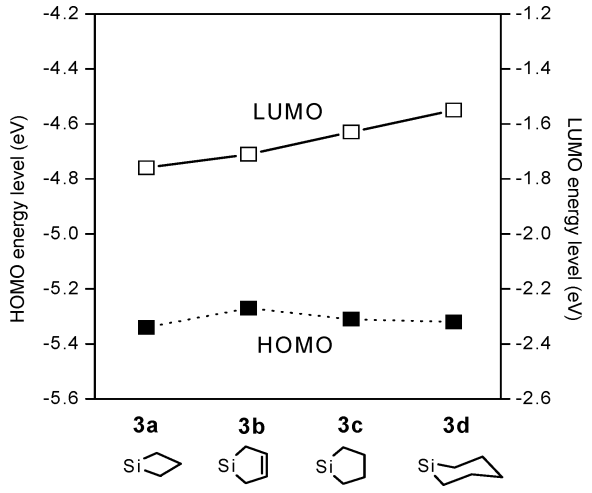

Figure 6. HOMO and LUMO energy levels of silacycloalkylsiloles (**3**) calculated at the RHF/6-31G level of theory.

silacycloalkyl ring increases, whereas the HOMO levels are comparable to each other. In addition, the gradual elevation of the LUMO levels with increasing exocyclic ring size (Figure 9) provides direct evidence for the occurrence of the blue shift observed in both UV and PL spectra. It has been suggested by Tamao that based on atomic size difference, the incorporation of heteroatoms into the silicon position in the silole alters the electronic structure of the corresponding heteroles.[13]

Theoretical Study of the Electronic Structures of Silole Derivatives (3). In order to evaluate the changes in the electronic structures induced by varying the size of the exocyclic silacycloalkyl ring, we carried out ab initio calculations on the siloles (**3**). The calculations were performed using the Hartreec−Fock (HF) approximation with the Gaussian 98 program.[15] The geometries of **3** were fully optimized using the 6-31G basis set. No atoms were omitted from the detailed investigation of the bond lengths and angles of the optimized structure. The results of the calculations are summarized in Table 5.

Consistent with the energy level data obtained in the CV experiments, the ab initio calculations revealed a distinctive systematic increase in the LUMO energy levels of the four siloles, but no change in the HOMO energy levels (Figure 6). Previously, Yamaguchi et al.[13] elaborated the relationship between the geometries of metalloles and the corresponding electronic structures and found that the LUMO levels, but not the HOMO levels, were susceptible to geometric changes. Similar geometries and electronic-state relationships were observed in the silole series synthesized in the present work. As shown in Table 5, the LUMO energy levels significantly depend on the Si−$C_1(C_2)$ bond lengths and C_1−Si−C_2 bond angles. The LUMO energy levels increase in the order **3a** < **3b** < **3c** < **3d** as the Si−$C_1(C_2)$ bond lengths increase and the C_1−Si−C_2 bond angle decreases. These optimized structural parameters establish that the elongated Si−C distances induce a weakening of the orbital interaction between the π^* orbital of the butadiene moiety and the σ^* orbital of the exocyclic silicon ring, such that the overall LUMO level of the siloles (**3**) increases with increasing ring size (Figure 7). In addition, σ^* orbital energy levels of the exocyclic silacycloalkyl ring were estimated by the ab initio calculations for *Cy*SiH_2 (*Cy* = silacycloalkyl rings), the results being shown in Figure 8. Consistent with our expectation, the elevation in the σ^* orbital energy levels by releasing strain in the exocyclic silacycloalkyl ring is observed, which would result in the less effective σ^*−π^* interaction. However, a slight irregularity was observed in the LUMO level for **3b** (Figure 8).

Electroluminescent Devices. It has been noted that the 2,3,4,5-tetraphenyl silole derivatives can be used as potential

(13) Yamaguchi, S.; Itami, Y.; Tamao, K. *Organometallics* **1998**, *17*, 4910.

(14) Anderson, J. D.; McDonald, E. M.; Lee, P. A.; Anderson, M. L.; Ritchie, E. L.; Hall, H. K.; Hopkins, T.; Padias, A.; Thayumanavan, S.; Barlow, S.; Marder, S. R.; Jabbour, G. E.; Shaheen, S.; Kippelen, B.; Peyghambarian, N.; Wightman, R. M.; Armstrong, N. R.; Mash, E. A.; Wang, J. *J. Am. Chem. Soc.* **1998**, *120*, 9646.

(15) Frisch, M. J.; Trucks, G. W.; Schlegel, H. B.; Scuseria, G. E.; Robb, M. A.; Cheeseman, J. R.; Zakrzewski, V. G.; Montgomery, J. A., Jr.; Stratmann, R. E.; Burant, J. C.; Dapprich, S.; Millam, J. M.; Daniels, A. D.; Kudin, K. N.; Strain, M. C.; Farkas, O.; Tomasi, J.; Barone, V.; Cossi, M.; Cammi, R.; Mennucci, B.; Pomelli, C.; Adamo, C.; Clifford, S.; Ochterski, J.; Petersson, G. A.; Ayala, P. Y.; Cui, Q.; Morokuma, Q.; Malick, D. K.; Rabuck, A. D.; Raghavachari, K.; Foresman, J. B.; Cioslowski, J.; Ortiz, J. V.; Baboul, A. G.; Stefanov, B. B.; Liu, G.; Liashenko, A.; Piskorz, P.; Komaromi, I.; Gomperts, R.; Martin, R. L.; Fox, D. J.; Keith, T.; Al-Laham, M. A.; Peng, C. Y.; Nanayakkara, A.; Gonzalez, C.; Challacombe, M.; Gill, P. M. W.; Johnson, B.; Chen, W.; Wong, M. W.; Andres, J. L.; Gonzalez, C.; Head-Gordon, M.; Replogle, E. S.; Pople, J. A. *Gaussian 98*; Gaussian, Inc.: Pittsburgh, PA, 1998.

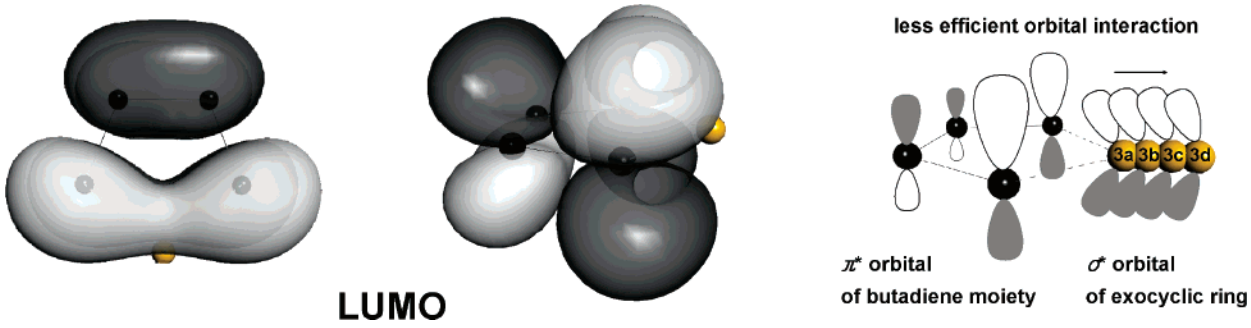

Figure 7. Change in the $\sigma^*-\pi^*$ orbital interaction with elongation of the Si−C distance.

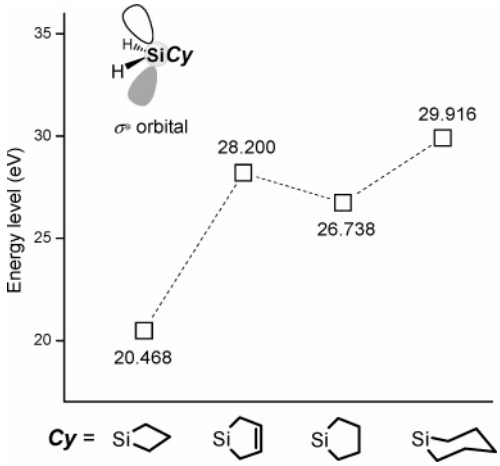

Figure 8. σ^* orbital levels of $CySiH_2$ (Cy = silacycloalkyl rings) based on ab initio calculation (RHF/6-31G).

emitting materials for the fabrication of organic light-emitting devices (OLEDs).[3] In particular, an electroluminescent (EL) device fabricated using **MePh** as an emitting layer showed excellent external EL quantum efficiency, reaching a value of 8%.[3d,f] On the basis of the preliminary DSC results, the newly synthesized series of exocyclic siloles may serve as better emitting materials than the corresponding acyclic siloles (including **MePh**). To test this, we fabricated standard EL devices in which the silacycloalkylsiloles (**3**) were used as the emitting materials. The EL devices were fabricated on ITO (indium tin oxide)-coated glass (20 Ω/sq) by the sequential vacuum evaporations of a *N*,*N*′-bis(1-naphthyl)-*N*,*N*′-diphenylbenzidine (NPB) hole-transport layer, a silole (**3**) emission layer, and a Alq_3 electron-transport layer, completed with a LiF/Al cathode layer. All of the EL spectra of **3** are overlapped with the PL spectra, implying that exciton formation occurs in the silole layer (Figure 11). The performance of the EL devices is summarized

Table 5. Calculated HOMO and LUMO Energy Levels and Optimized Geometries for Silacycloalkylsiloles (3)[a]

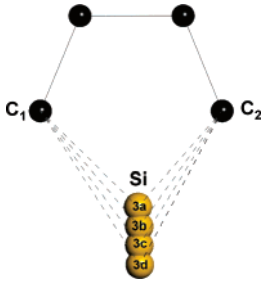

silole	HOMO (eV)	LUMO (eV)	Si−C_1(Si−C_2) (Å)	C_1−Si−C_2 (deg)
3a	−5.34	−1.76	1.9049(1.9073)	90.913
3b	−5.27	−1.71	1.9082	90.735
3c	−5.31	−1.63	1.9085	90.640
3d	−5.32	−1.55	1.9134(1.9100)	90.400

[a] HOMO−LUMO energy levels and geometries were fully optimized at the RHF/6-31G level of theory.

in Table 6. The general trend of the observed changes in the LUMO energy level, as a result of the variation of the exocyclic ring size, is further illustrated by the EL characteristics. As shown in Figure 10, the four-membered silacyclobutyl exocyclic ring silole **3a** showed the lowest turn-on voltage in the corresponding $I-V$ curves, indicating the lowest LUMO energy level. However, with the exception of the silacyclopentyl silole (**3c**), the brightness of the other siloles studied decayed rapidly as the voltage was increased. This behavior is due to the quality of the silole films. To evaluate the relative stability of the silole films, each of the siloles (**3**) was vapor-deposited onto bare ITO and exposed to humid ambient air for 12 h. The results of this test were as follows: the silacyclohexyl silole (**3d**) formed polycrystals on the ITO surface; the silacyclobutyl (**3a**) and -pentenyl (**3b**) siloles showed poor-quality opaque films with a

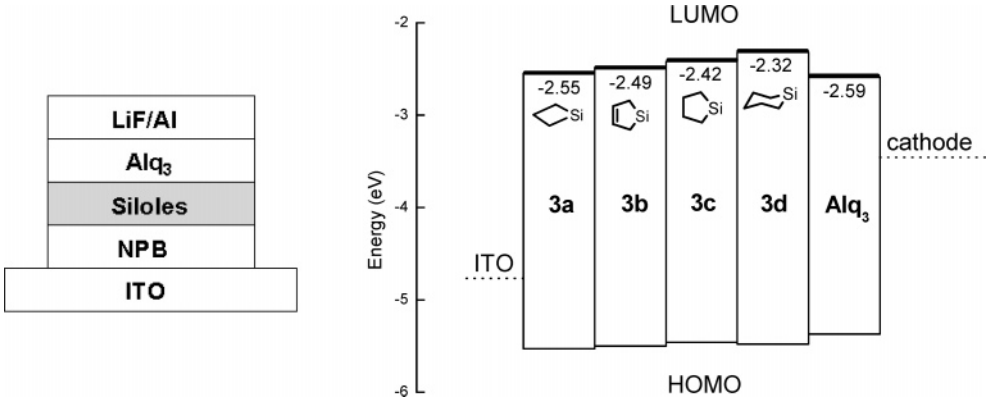

Figure 9. Device structure and HOMO−LUMO levels estimated from cyclic voltammograms.

Table 6. EL Spectral Data and Performance Characteristics of Devices[a]

silole	CIE coordinates (x, y)[b]	EL emission λ_{max} (nm)[b]	max. luminance (cd/m^2)	max. current efficiency (cd/A)	turn-on voltage (V)[c]
3a	(0.25, 0.44)	510	860	0.20	3.7
3b	(0.23, 0.41)	500	2160	0.76	4.9
3c	(0.22, 0.39)	495	11 000	3.96	4.6
3d	(0.16, 0.30)	485	810	1.38	6.6
MePh	(0.24, 0.39)	495	9100	3.34	5.7

[a] Device structure: ITO/NPB (50 nm)/siloles (40 nm)/Alq_3 (10 nm)/LiF (0.5 nm)/Al (120 nm). [b]Determined from the EL spectra (Figure 11). [c]Defined as the voltage required to give a current density of 1 mA/cm^2.

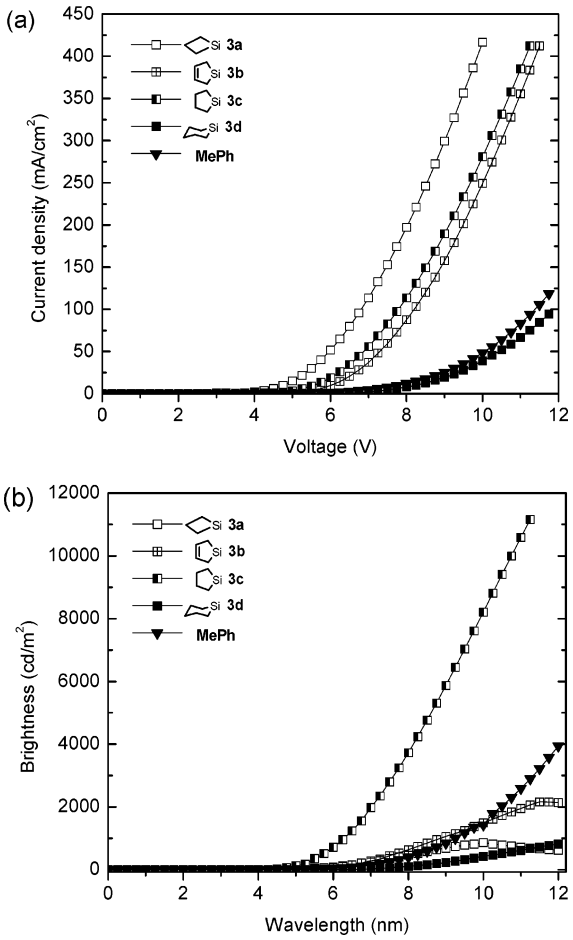

Figure 10. (a) Current density vs voltage ($I-V$) characteristics and (b) brightness vs voltage ($L-V$) for the devices using silacycloalkylsiloles (**3**) or **MePh** as an emitting layer.

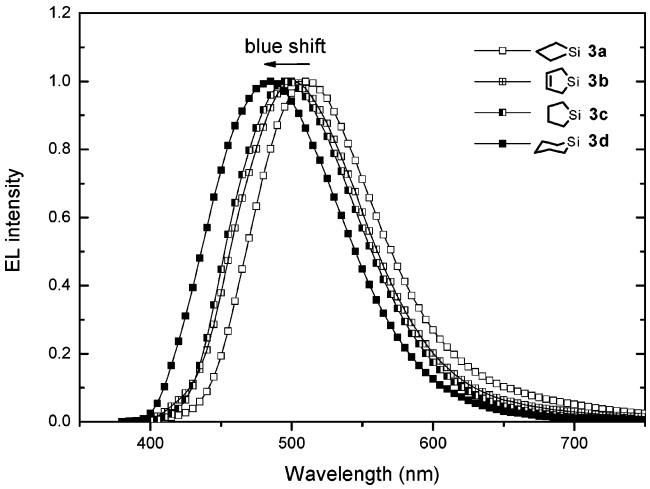

Figure 11. EL spectra of the devices based on the silacycloalkylsiloles (**3**).

droplet-like morphology, rather than being transparent and amorphous; and, as expected, the silacyclopentyl silole (**3c**) exhibited the most stable film quality. Moreover, **3c** also exhibited a maximum brightness of 11 000 cd/cm^2 at 11 V and a current efficiency of 3.96 cd/A at 10 mA/cm^2, which are superior to the corresponding values for the device based on **MePh** (Table 6). Therefore, we suggest that one reason for the enhanced performance of **3c** is its increased thermal stability resulting from cyclization of the exocyclic ring, as well as from the stability of the thin film, giving rise to a marked enhancement of the luminance and its efficiency.

Conclusion

Here we have described the synthesis of a new class of electroluminescent compounds based on tetraphenylsiloles with 1,1′-silacycloalkyl substituents, prepared using a lithium diyne procedure. Compared with known acyclic silole derivatives, these siloles showed enhanced thermal stability in DSC experiments, which can be ascribed to their rigid structures. The geometric nature of the silacycloalkyl substituent induced a characteristic blue shift in the photophysical experiments of the resulting silole complex. To determine the origin of the characteristic effects, cyclic voltammetry experiments and theoretical calculations were carried out. The results showed that the LUMO level of the siloles is finely controlled by the geometry of the exocyclic ring. In an EL device fabricated using **3** as the emissive layer, the silacyclopentyl silole (**3c**) showed the best performance among the prepared siloles (including **MePh**) due to its thermal stability and good film morphology. These results indicate that the silole **3c** is a promising emitting material for the preparation of electroluminophores with predictable photophysical properties. Efforts toward the investigation of the solid-state luminescence, fabrication, and evaluation of OLEDs utilizing compounds **3** are currently underway.

Experimental Section

General Procedures. All manipulations were performed under a dry nitrogen or argon atmosphere using standard Schlenk techniques. THF was freshly distilled over potassium benzophenone. ^{1}H and ^{13}C spectra were recorded on a Varian unity Inova AS600 spectrometer operating at 599.80 and 150.83 MHz, respectively. All proton and carbon chemical shifts were measured relative to internal residual benzene from the lock solvent (99.9% $CDCl_3$) and then referenced to Me_4Si (0.00 ppm). The elemental analyses were performed with a Carlo Erba Instruments CHNS-O EA 1108 analyzer. High-resolution tandem mass spectrometry (Jeol LTD JMS-HX 110/110A) was performed by the Daejon Branch of the Korean Basic Science Institute. The absorption and photoluminescence spectra were recorded on a Shimadzu UV-3101PC UV−vis−NIR scanning spectrophotometer and a Varian Cary Eclipse fluorescence spectrophotometer, respectively. The fluorescence quantum yields in chloroform using 9,10-diphenylanthracene as a standard were determined by the dilution method. The fluorescence

decay curves were recorded on a PTI fluorescence Master 2M1 luminescence spectrophotometer using a PTIG2-3300 nitrogen laser for excitation. Cyclic yvoltammetry (CV) experiments were performed using a BAS 100 electrochemical analyzer. Platinum, wire, and $Ag/AgNO_3$ (0.10 M) were used as the working, counter, and reference electrodes, respectively. The CV experiments were performed using these three electrodes immersed in a solution of 0.1 M tetrabutylammonium perchlorate (Bu_4NClO_4) in anhydrous CH_2Cl_2 at room temperature under argon with a scan rate of 0.1 V/s. The thermal stability of the siloles (**3**) was measured using differential scanning calorimetry (SETRAM TG-DTA/DSC). A heating rate of 20 °C/min was used after first melting the compound, and this was subsequently followed by rapid cooling to room temperature. Diphenylacetylene and lithium were both purchased from Aldrich and used without further purification. Silacyclobutyl dichloride (**1a**), silacyclopentenyl dichloride (**1b**), silacyclopentyl dichloride (**1c**), and silacyclohexyl dichloride (**1d**) were all prepared according to literature methods.[16]

Synthesis of 2,3,4,5-Tetraphenylsilole with an Exocyclic Silacyclobutyl Ring (3a). Clean lithium shavings (175 mg, 25 mmol) were added to a solution of diphenylacetylene (2.25 g, 12.5 mmol) in dry THF (10 mL). The reaction mixture was stirred at room temperature for 2 h in a dry argon atmosphere. The mixture was diluted with 120 mL of THF, followed by the addition of silacyclobutyl dichloride (**1a**) (0.88 g, 6.25 mmol). After heating at reflux for 6 h, the mixture was filtered through a pad of Celite and washed with brine. The organic layer was extracted with CH_2Cl_2 and dried over $MgSO_4$. The volatile solvent was removed under reduced pressure, and the residue was purified by flash chromatography over silica gel using 10% diethyl ether in hexane as an eluent. Recrystallization from diethyl ether at 0 °C produced **3a** as a greenish-yellow powder. Yield: 1.59 g (60%). Mp: 172 °C. ^{1}H NMR ($CDCl_3$): δ 7.17 (m, 4H, *Ph*), 7.09 (m, 6H, *Ph*), 7.01 (m, 6H, *Ph*), 6.80 (m, 4H, *Ph*), 2.25 (m, 2H, $SiCH_2CH_2$, $^3J_{H-H} = 8.4$ Hz), 1.60 (t, 4H, $SiCH_2CH_2$, $^3J_{H-H} = 8.4$ Hz). ^{13}C NMR ($CDCl_3$): δ 154.99, 139.72, 138.47, 137.93, 130.11, 129.19, 128.21, 127.62, 126.60, 125.93, 19.76 ($SiCH_2CH_2$), 13.68 ($SiCH_2CH_2$). FAB-MS calcd for $[C_{31}H_{26}Si]^+$: 426.635. Found: 426.109. Anal. Calcd for $C_{31}H_{26}Si$: C, 87.27; H, 6.14. Found: C, 87.02; H, 6.13.

Synthesis of 2,3,4,5-Tetraphenylsilole with an Exocyclic Silacyclopentenyl Ring (3b). This compound was prepared by a procedure similar to that of **3a**, using silacyclopentenyl dichloride (**1b**) instead of silacyclobutyl dichloride (**1a**); the product (**3b**) was isolated as a green solid. Yield: 1.5 g (55%). Mp: 215 °C. ^{1}H NMR ($CDCl_3$): δ 7.11 (m, 4H, *Ph*), 7.05 (m, 8H, *Ph*), 6.92 (m, 4H, *Ph*), 6.86 (m, 4H, *Ph*), 6.09 (s, 2H, $SiCH_2CH$), 1.85 (s, 4H, $SiCH_2CH$). ^{13}C NMR ($CDCl_3$): δ 155.62, 139.23, 139.18, 139.06, 132.00 ($SiCH_2CH$), 130.05, 129.32, 128.20, 127.83, 126.65, 126.08, 15.05 ($SiCH_2CH$). FAB-MS calcd for $[C_{32}H_{26}Si]^+$: 438.646. Found: 438.040. Anal. Calcd for $C_{32}H_{26}Si$: C, 87.62; H, 5.97. Found: C, 87.97; H, 6.00.

Synthesis of 2,3,4,5-Tetraphenylsilole with an Exocyclic Silacyclopentyl Ring (3c). This compound was prepared by a procedure similar to that of **3a**, using silacyclopentyl dichloride (**1c**) instead of silacyclobutyl dichloride (**1a**); the product was isolated as a green crystalline solid. Yield: 1.43 g (52%). Mp: 220 °C. ^{1}H NMR ($CDCl_3$): δ 7.12 (m, 4H, *Ph*), 7.02 (m, 8H, *Ph*), 6.90 (m, 4H, *Ph*), 6.81 (m, 4H, *Ph*), 1.76 (m, 4H, $SiCH_2CH_2$), 1.08 (m, 4H, $SiCH_2CH_2$). ^{13}C NMR ($CDCl_3$): δ 155.05, 140.35, 139.92, 138.91, 130.23, 129.15, 128.14, 127.59, 126.45, 125.76, 28.18 ($SiCH_2CH_2$), 10.28 ($SiCH_2CH_2$). FAB-MS calcd for $[C_{32}H_{28}Si]^+$: 440.662. Found: 440.082. Anal. Calcd for $C_{32}H_{28}Si$: C, 87.22; H, 6.40. Found: C, 86.91; H, 6.39.

Synthesis of 2,3,4,5-Tetraphenylsilole with an Exocyclic Silacyclohexyl Ring (3d). This compound was prepared by a procedure similar to that of **3a**, using silacyclohexyl dichloride (**1d**) instead of silacyclobutyl dichloride (**1a**); the product was isolated as a greenish-blue solid. Yield: 1.33 g (47%). Mp: 208 °C. ^{1}H NMR ($CDCl_3$): δ 7.16 (m, 4H, *Ph*), 7.07 (m, 2H, *Ph*), 6.98 (m, 10H, *Ph*), 6.79 (m, 4H, *Ph*), 1.70 (m, 4H, $SiCH_2CH_2CH_2$), 1.44 (m, 2H, $CH_2CH_2CH_2$), 1.12 (t, 4H, $SiCH_2CH_2CH_2$, $^3J_{H-H} = 6.6$ Hz). ^{13}C NMR ($CDCl_3$): δ 154.62, 142.54, 140.96, 138.75, 130.30, 129.07, 128.09, 127.40, 126.29, 125.53, 29.51 ($CH_2CH_2CH_2$), 24.61 ($SiCH_2CH_2CH_2$), 10.16 ($SiCH_2CH_2CH_2$). FAB-MS calcd for $[C_{33}H_{30}Si]^+$: 454.689. Found: 454.011. Anal. Calcd for $C_{33}H_{30}Si$: C, 87.17; H, 6.65. Found: C, 86.93; H, 6.63.

Fabrication of EL Devices. The anode, ITO, with a resistance of 10 Ω/sq, was patterned using photolithography and wet etching processes. The organic and metal cathode layers were deposited sequentially through a shadow mask by thermal evaporation with a background pressure of 10^{-7} Torr and a deposition rate of 1−2 Å/s. The fabricated devices were encapsulated with a glass cap and UV sealant. All the devices had an emitting area of 0.4×0.6 mm^2. A spectro-radiometer (Minolta CS1000) was employed for measurements of the electroluminescence spectra. The current−voltage ($I-V$) characteristics were measured with an experimental setup consisting of a Keithley 2400 source meter equipped with a calibrated photodiode. The measurements and data acquisition were controlled using LabVIEW (National Instrument) software.

Acknowledgment. This work was supported by a Grant (No. R02-2004-000-10095-0) from the Basic Research Program of the Korea Science and Engineering Foundation.

Supporting Information Available: ^{1}H and ^{13}C NMR spectroscopic data for **3**. This material is available free of charge via the Internet at http://pubs.acs.org.

OM060854D

(16) Kim, S.-J.; Jung, I. N.; Yoo, B. R.; Cho, S.; Ko, J.; Kim, S. H.; Byun, D.; Kang, S. O. *Organometallics* **2001**, *20*, 2136.